The NV^{-}....N^{+} charged pair in Diamond: a Quantum-Mechanical investigation

Anna M. Ferrari[a,*], Khaled E. El-Kelany[b,a,*], Francesco S. Gentile[c], Maddalena D'Amore[a], Roberto Dovesi[c]

[a] *Dipartimento di Chimica, Università di Torino and NIS (Nanostructured Interfaces and Surfaces) Centre, Via P. Giuria 5, 10125 Torino, Italy*
[b] *Institute of Nanoscience and Nanotechnology, Kafrelsheikh University, 33516 Kafrelskiekh, Egypt*
[c] *Dipartimento di Chimica, Università di Torino Centre, Via P. Giuria 5, 10125 Torino, Italy*

Supplementary Materials

*Corresponding author
Email addresses: anna.ferrari@unito.it (Anna M. Ferrari), khaled_elkelany@nano.kfs.edu.eg (Khaled E. El-Kelany)

1. Computational Details

In this section we summarize some of the computational details that are not specific of the present manuscript, but are common to many of the recent publications by the present authors and collaborators, and describing the properties of defects in diamond and silicon.

The truncation criteria of the Coulomb and exchange infinite lattice series are controlled by five thresholds, T_i, which have been set to 8 (T_1-T_4) and 16 (T_5). The convergence tolerance on energy for the SCF step has been set to 10^{-8} E_h for structural optimizations, and to 10^{-10} E_h for frequency calculations.
The DFT exchange-correlation contribution and its gradient are evaluated by numerical integration over the unit cell volume. The generation of the integration grid points is based on an atomic partition method, originally proposed by Becke[1], in which the radial and angular points are obtained from Gauss-Legendre quadrature and Lebedev two-dimensional distributions respectively. The choice of a suitable grid is crucial both for numerical accuracy and cost consideration. In this study a pruned grid with 75 radial and 974 angular points has been used.
Reciprocal space sampling is based on a regular Pack-Monkhorst[2] sub-lattice grid centered at the Γ point (*i.e.* at the center of the first Brillouin zone), that leads to 2 sample points along each of the reciprocal lattice vectors, which corresponds to 4 and 6 **k**-points for C_{3v} and C_S symmetry, respectively, in the irreducible part of the Brillouin zone, after point symmetry has been taken into account.

Harmonic phonon frequencies, ω_p at the Γ point were obtained by diagonalization of the mass-weighted Hessian matrix of second energy derivatives with respect to atomic displacements u:[3, 4, 5, 6, 7]

$$W^{\Gamma}_{ai,bj} = \frac{H^{\mathbf{0}}_{ai,bj}}{\sqrt{M_a M_b}} \quad \text{with} \quad H^{\mathbf{0}}_{ai,bj} = \left(\frac{\partial^2 E}{\partial u^{\mathbf{0}}_{ai} \partial u^{\mathbf{0}}_{bj}} \right) \,, \tag{1}$$

where atoms a and b (with atomic masses M_a and M_b) in the reference cell, $\mathbf{0}$, are displaced along the i-th and j-th Cartesian directions, respectively. First order derivatives are computed analytically, whereas second order derivatives are obtained numerically, using a two-point formula (as the difference of the gradient at the equilibrium position, and after a displacement of 0.003 Å along each cartesian coordinate; note that as the optimization of the structure is a numerical process, the gradient at equilibrium is not exactly null, but simply lower than the threshold of the optimizer.
Integrated intensities for IR absorption $\mathcal{I}_p$ were computed for each normal mode Q_p from the mass-weighted effective-mode Born-charge vector $\vec{Z}_p$ [8, 9] using a CPHF/KS analytical method:[10]

$$\mathcal{I}_p \propto \left| \vec{Z}_p \right|^2 \text{ with } \quad \vec{Z}_p = \frac{\partial \vec{\mu}}{\partial Q_p}. \tag{2}$$

2. Figures

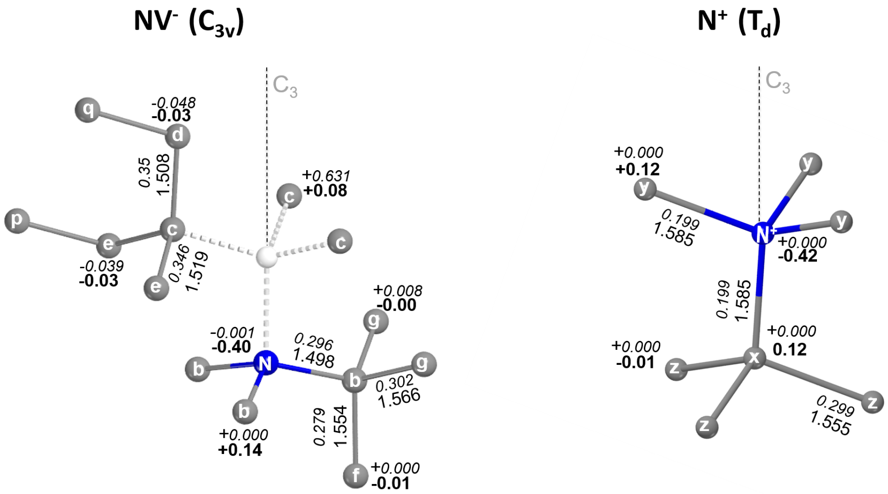

Figure 1: Properties of the NV^- (C_{3v} symmetry) and N^+ (T_d symmetry) defects obtained with the S_{216} supercell at the B3LYP/6-21G level and adopting the CC model. Mulliken net charges and spin momenta (in $|e|$, **bold** and *italic* respectively) are reported for each symmetry irreducible atom. Bond distances (in Å) and Mulliken bond populations (in $|e|$, *italic*) are reported below each pair of atoms.

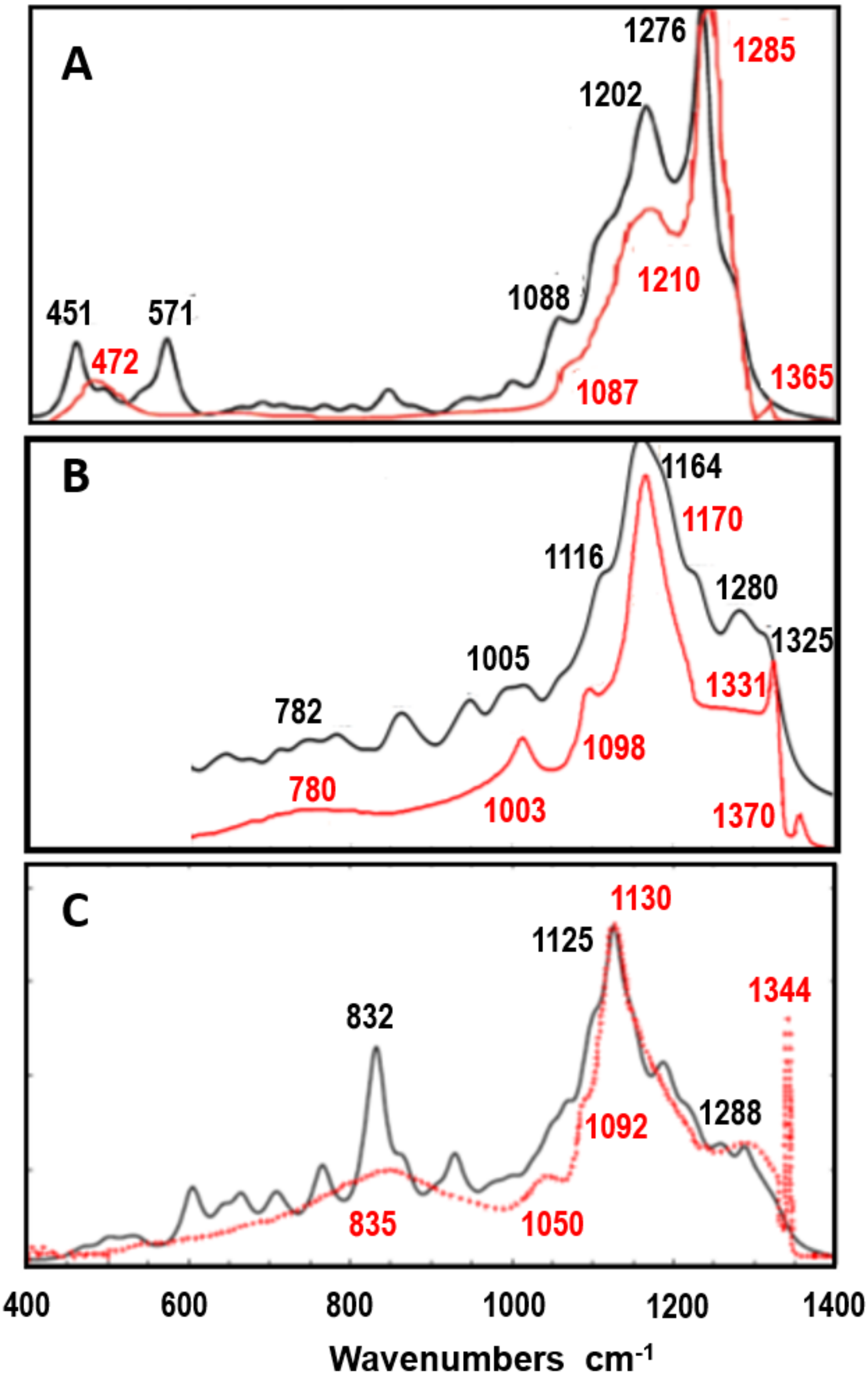

Figure 2: IR spetra of diamond containing N defects. A, A defect (a couple of substitutional vicinal N atoms); B, the B defect (a vacancy V surrounded by 4 N atoms); C, the C defect (a single substitutional N atom, N^+ defect).

3. Tables

Table 1: Bond distance (in Å), Mulliken atomic charges (in $|e|$), and spin densities (in $|e|$) for the triplet state of NV^-...N^+ defect. The results of the S_{64}, S_{216}, and S_{512} supercells are reported. The data refer to the negative part of the double defect. For comparison, the data of the isolated NV^- and NV^0 centers are also reported in the last two columns, obtained with the S_{216} supercell.

	NV^-...N^+			NV^-	NV^0
	S_{64}	S_{216}	S_{512}		
d(N-N^+)	6.228	7.956	12.334	-	-
d(N-$C_{(b)}$)	1.497	1.497	1.498	1.501	1.525
d($C_{(b)}$-$C_{(f)}$)	1.553	1.554	1.554	1.557	1.560
d($C_{(b)}$-$C_{(g)}$)	1.565	1.566	1.566	1.569	1.564
d($C_{(c)}$-$C_{(e)}$)	1.517	1.519	1.519	1.521	1.507
d($C_{(c)}$-$C_{(d)}$)	1.510	1.509	1.508	1.510	1.514
q(N)	-0.40	-0.40	-0.40	-0.40	-0.38
q($C_{(b)}$)	+0.14	+0.14	+0.14	+0.13	+0.12
q($C_{(c)}$)	+0.08	+0.08	+0.08	+0.07	+0.09
q($C_{(d)}$)	-0.03	-0.03	-0.03	-0.04	-0.04
q($C_{(e)}$)	-0.03	-0.03	-0.03	-0.04	-0.04
q($C_{(f)}$)	0.00	0.00	0.00	-0.01	0.00
q($C_{(g)}$)	0.00	0.00	0.00	0.00	0.00
q($C_{(p)}$)	+0.004	+0.003	+0.003	+0.003	+0.001
q($C_{(q)}$)	-0.006	+0.001	+0.002	+0.002	+0.001
μ(N)	0.001	-0.001	-0.001	0.000	0.154
μ($C_{(b)}$)	+0.001	0.000	0.000	0.000	-0.007
μ($C_{(c)}$)	+0.632	+0.632	+0.631	+0.632	+0.883
μ($C_{(d)}$)	-0.048	-0.048	-0.048	-0.048	-0.058
μ($C_{(e)}$)	-0.039	-0.039	-0.039	-0.039	-0.062
μ($C_{(f)}$)	+0.002	0.000	0.000	0.000	+0.010
μ($C_{(g)}$)	+0.011	+0.008	+0.008	+0.008	+0.012
μ($C_{(p)}$)	+0.034	+0.034	+0.034	+0.034	+0.053
μ($C_{(q)}$)	+0.041	+0.038	+0.038	+0.038	+0.054

Table 2: Bond distance (in Å), Mulliken atomic charges (in $|e|$), and spin densities (in $|e|$) for the positively charged part of the NV^-...N^+ defect are reported iand compared with the isolated $N^+(T_d)$ center.

	$NV^-...N^+$			$N^+(T_d)$
	S_{64}	S_{216}	S_{512}	
$d(N^+\text{-}C_{(x)})$	1.584	1.585	1.585	1.582
$d(N^+\text{-}C_{y)})$	1.587	1.585	1.585	1.582
$d(C_{(x)}\text{-}C_{(z)})$	1.559	1.555	1.555	1.553
$q(N^+)$	-0.42	-0.42	-0.42	-0.42
$q(C_{(x)})$	0.12	0.12	0.12	0.12
$q(C_{(y)})$	0.12	0.12	0.12	0.12
$\mu(N^+)$	0.011	0.000	0.000	0.000
$\mu(C_{(x)})$	-0.002	0.000	0.000	0.000
$\mu(C_{(y)})$	-0.006	0.000	0.000	0.000

Table 3: Net atomic charges (in $|e|$) of the defect atoms for the negatively charged part of the NV^{-}-N^{+} center. m refers to the multiplicity; R indicates the distance in Å between the given atom and the vacancy center. Values in parentheses refer to Hirshfield charges. The sum of the charges of a given shell is also reported. The comparison with the NV^{-} and NV^{0} defects is also considered.

site	m	R	$NV^{-} \ldots N^{+}$		NV^{-}	NV^{0}
			S_{216}	S_{512}		
N	1	~1.71	-0.395	-0.395	-0.398	-0.384
			(-0.257)	(-0.255)	(-0.263)	(-0.197)
$C_{(c)}$	3	~1.64	+0.077	+0.078	+0.069	+0.092
			(-0.204)	(-0.202)	(-0.210)	(-0.089)
Sum *Shell* 1			-0.164	-0.161	-0.191	-0.108
4-*atoms*			(-0.869)	(-0.861)	(-0.881)	(-0.464)
$C_{(e)}$	6	~2.52	-0.031	-0.031	-0.035	-0.038
			(+0.056)	(+0.055)	(+0.054)	(+0.026)
$C_{(b)}$	3	~2.55	+0.139	+0.138	+0.132	+0.123
			(+0.161)	(+0.157)	(+0.156)	(+0.133)
$C_{(d)}$	3	~2.55	-0.030	-0.030	-0.034	-0.038
			(+0.050)	(+0.048)	(+0.047)	(+0.026)
Sum *Shell* 2			+0.141	+0.138	+0.084	+0.027
12-*atoms*			(+0.969)	(+0.945)	(+0.933)	(+0.633)
$C_{(i)}$	3	~2.97	+0.006	+0.005	+0.001	+0.006
			(-0.002)	(-0.002)	(-0.007)	(+0.005)
$C_{(g)}$	6		+0.002	+0.002	-0.002	+0.001
			(-0.023)	(-0.021)	(-0.027)	(-0.017)
$C_{(h)}$	3		+0.008	+0.008	+0.003	+0.007
			(+0.002)	(+0.003)	(-0.002)	(+0.004)
Sum *Shell* 3			+0.054	+0.051	0.000	+0.048
12-*atoms*			(-0.132)	(-0.123)	(-0.189)	(-0.075)
Sum			+0.031	+0.028	-0.107	-0.033
Shells 1, 2, 3			(-0.038)	(-0.039)	(-0.137)	(+0.094)
$C_{(m)}$	3	~3.60	-0.007	-0.007	-0.012	-0.006
			(+0.005)	(+0.004)	(+0.002)	(+0.002)
$C_{(l)}$	3		-0.003	-0.003	-0.008	-0.005
			(+0.005)	(+0.004)	(+0.002)	(+0.000)
$C_{(p)}$	3	~3.95	+0.001	+0.002	-0.003	+0.006
			(-0.016)	(-0.014)	(-0.019)	(-0.002)
$C_{(q)}$	6		+0.003	+0.003	-0.002	+0.006
			(-0.014)	(-0.014)	(-0.018)	(-0.001)
$C_{(f)}$	3		-0.005	-0.004	-0.009	-0.004
			(-0.063)	(-0.055)	(-0.061)	(-0.041)
Sum *Shell* 4			-0.027	-0.018	-0.108	+0.009
18-*atoms*			(-0.291)	(-0.267)	(-0.336)	(-0.129)
Sum			+0.004	+0.010	-0.215	-0.024
Shells 1, 2, 3, 4			(-0.329)	(-0.306)	(-0.473)	(-0.035)
Sum *Shell* 5		~4.40		-0.006		
24-*atoms*				(+0.018)		
Sum *Shell* 6		~4.68		+0.008		
16-*atoms*				(-0.008)		
Sum *Shell* 7		~5.10		-0.027		
12-*atoms*				(0.000)		
Sum				-0.015		
Shells 1, 2, 3, 4, 5, 6, 7				(-0.296)		

Table 4: Net atomic charges (in $|e|$) in the positively charged part of the NV^{-}-N^{+} center. m is the multiplicity, R indicates the distance in Å between the given atom and the vacancy center. Values in parentheses refer to Hirshfield charges. The sum of the charges in a given shell is also reported. Also the data for the pure $N^{+}(T_d)$ defect are shown.

site	m	R	$NV^{-} \ldots N^{+}$ S_{216}	$NV^{-} \ldots N^{+}$ S_{512}	$N^{+}(T_d)$
N^{+}	1	0.00	-0.419 (+0.061)	-0.419 (+0.063)	-0.420 (+0.071)
$C_{(x)}$	4	~1.59	+0.119 (+0.102)	+0.118 (+0.101)	+0.124 (+0.101)
$C_{(y)}$	12	~2.55	-0.010 (-0.032)	-0.009 (-0.029)	-0.004 (-0.022)
$C_{(z)}$	12	~2.99	0.000 (+0.005)	0.000 (+0.004)	+0.005 (+0.005)
Sum *Shell* 1 30-*atoms*			-0.063 (+0.145)	-0.055 (+0.167)	+0.088 (+0.271)
Sum *Shell* 2	6	~3.60		-0.003 (-0.021)	
Sum *Shell* 3	12	~3.93		+0.009 (+0.108)	
Sum *Shell* 4	24	~4.41		-0.006 (-0.045)	
Sum *Shell* 5	16	~4.68		+0.007 (+0.005)	
Sum *Shell* 6	12	~5.09		+0.006 (+0.003)	
Sum Shells 1, 2, 3, 4, 5, 6				-0.042 (+0.217)	

References

[1] A. D. Becke, A Multicenter Numerical Integration Scheme for Polyatomic Molecules, J. Chem. Phys. 88 (4) (1988) 2547–2553.

[2] H. J. Monkhorst, J. D. Pack, Special Points for Brillouin-Zone Integrations, Phys. Rev. B 13 (12) (1976) 5188.

[3] F. Pascale, C. M. Zicovich-Wilson, F. L. Gejo, B. Civalleri, R. Orlando, R. Dovesi, The Calculation of the Vibrational Frequencies of the Crystalline Compounds and its Implementation in the CRYSTAL Code, J. Comput. Chem. 25 (6) (2004) 888–897.

[4] C. M. Zicovich-Wilson, F. Pascale, C. Roetti, V. R. Saunders, R. Orlando, R. Dovesi, Calculation of the Vibration Frequencies of α-Quartz: The Effect of Hamiltonian and Basis Set, J. Comput. Chem. 25 (15) (2004) 1873–1881.

[5] A. Erba, M. Ferrabone, R. Orlando, R. Dovesi, Accurate Dynamical Structure Factors from *Ab Initio* Lattice Dynamics: The case of Crystalline Silicon, J. Comput. Chem. 34 (2013) 346–354.

[6] C. Carteret, M. De La Pierre, M. Dossot, F. Pascale, A. Erba, R. Dovesi, The Vibrational Spectrum of $CaCO_3$ Aragonite: a Combined Experimental and Quantum-Mechanical Investigation, J. Chem. Phys. 138 (1) (2013) 014201.

[7] J. Baima, M. Ferrabone, R. Orlando, A. Erba, R. Dovesi, Thermodynamics and Phonon Dispersion of Pyrope and Grossular Silicate Garnets from *Ab Initio* Simulations, Phys. Chem. Minerals 43 (2016) 137–149.

[8] G. M. Barrow, Introduction to Molecular Spectroscopy, McGraw-Hill, New York, 1962.

[9] B. A. Hess, L. J. Schaad, P. Carsky, R. Zahradnik, *Ab Initio* Calculations of Vibrational Spectra and Their Use in the Identification of Unusual Molecules, Chem. Rev. 86 (1986) 709–730.

[10] L. Maschio, B. Kirtman, R. Orlando, M. Rérat, *Ab Initio* Analytical Infrared Intensities for Periodic Systems Through a Coupled Perturbed Hartree-Fock/Kohn-Sham Method, J. Chem. Phys. 137 (20) (2012) 204113.